Comprehensive Structural Analysis of ZnTe and Mn-Doped ZnTe Thin Films

Ujjwal Prasad [a], Pushp Raj Harsh [a], S.R. Kumar [b], Kamal Prasad [a,*]

[a] *University Department of Physics, T.M. Bhagalpur University, Bhagalpur - 812007, India*

[b] *Department of Applied Science and Humanities, NIAMT, Hatia, Ranchi - 834003, India*

Editor's note: Modifying structural properties of II–VI semiconductors such as zinc telluride (ZnTe) with transition metal dopants like manganese (Mn) is key for advanced applications in spintronics and magnetic semiconductors. Prasad et al. analyzed ZnTe and Mn-doped ZnTe thin films using X-ray diffraction, confirming a cubic phase and revealing lattice distortion due to Mn doping. Techniques showed that Mn increases microstrain and internal stress while reducing crystallite size. These changes are crucial for enhancing the optical, electronic, and magnetic properties of ZnTe, making it suitable for optoelectronic and spintronic applications.

doi: 10.22034/jams.2026.260303

How to cite: U. Prasad et al., *Journal of Applied Material Science*, **2026**, *2*, 260303.

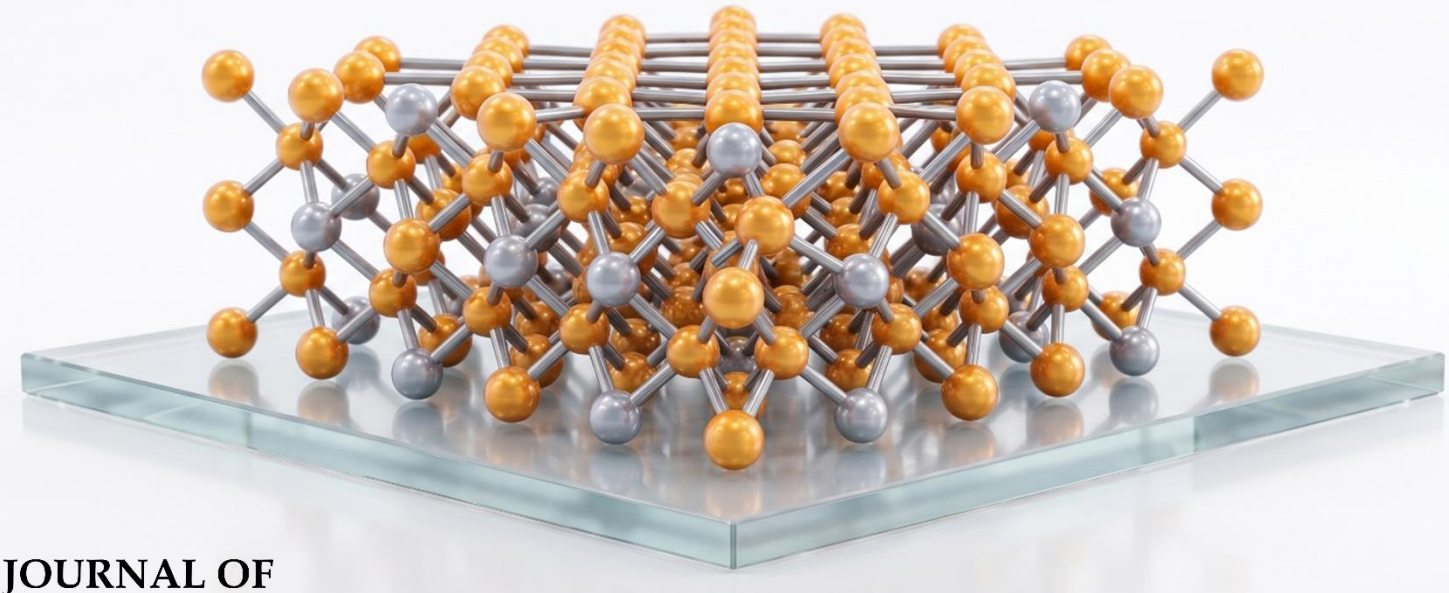

JOURNAL OF
APPLIED
MATERIAL
SCIENCE
jams.hsu.ac.ir

Journal of Applied Material Science **2026**, 2, 260303
How to cite: U. Prasad et al., *Journal of Applied Material Science*, **2026**, *2*, 260303.
Journal homepage: **jams.hsu.ac.ir**

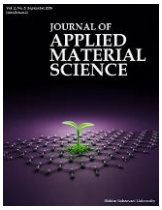

Original Research

Comprehensive Structural Analysis of ZnTe and Mn-Doped ZnTe Thin Films

Ujjwal Prasad [a], Pushp Raj Harsh [a], S.R. Kumar [b], Kamal Prasad [a,*]

[a] *University Department of Physics, T.M. Bhagalpur University, Bhagalpur - 812007, India*

[b] *Department of Applied Science and Humanities, NIAMT, Hatia, Ranchi - 834003, India*

Abstract

In this work, ZnTe and Mn-doped ZnTe thin films were synthesized and systematically analyzed for their structural properties. The cubic phase of ZnTe was confirmed by the X-ray diffraction (XRD) analysis, which also showed a minor shift in peak positions upon Mn doping, indicating lattice distortion. Several line profile analysis techniques, including the Scherrer method, Williamson–Hall models, Size–Strain Plot method, and Halder–Wagner approach, were used to assess the crystallite size and microstrain of the prepared thin films. The results consistently demonstrated that Mn-doping increased microstrain, internal stress, and energy density while decreasing crystallite size. The tendencies noted were further validated using the Halder-Wagner analysis, which offered better separation of size and strain factors. Increased microstrain and stored energy density imply that substantial internal distortions and lattice flaws are introduced by Mn inclusion. These structural modifications are critical for tailoring the optical, electronic, and magnetic properties of ZnTe thin films, making them ideal candidates for optoelectronic and spintronic applications.

Keywords: Semiconductor; ZnTe thin film; X-ray diffraction; Williamson–Hall; Halder-Wagner; Size-Strain Plot.

1. Introduction

II–VI compound semiconductor materials, especially ZnTe (zinc telluride), have garnered significant attention owing to its wide direct band gap (~2.26 eV at room temperature), high optical absorption coefficient, and excellent optoelectronic properties [1, 2]. These features make ZnTe a favorable candidate for applications in photovoltaics, laser diodes, and other optoelectronic devices. However, the ability to tailor the structural, electronic, and magnetic behavior of ZnTe is crucial for expanding its application range, especially in the emerging fields of spintronics and magnetic semiconductors. One effective strategy to modify the intrinsic properties of ZnTe is through the controlled incorporation of transition metal dopants such as manganese (Mn) [3]. Mn doping in ZnTe has been shown to introduce localized magnetic moments, alter

* Corresponding author.
Email address: prasad_k@tmbuniv.ac.in (K. Prasad)

Received 21 May 2026
Revised 14 July 2026
Accepted 7 August 2026
Available online 13 August 2026

https://doi.org/10.22034/jams.2026.260303

lattice parameters, and induce strain within the crystal structure [4]. Understanding how Mn incorporation influences the microstructure, particularly crystallite size, internal stress, lattice strain, and energy density, is therefore essential for optimizing the material's performance.

X-ray diffraction (XRD) is a powerful approach widely used to study the structural properties of thin films. Traditional approaches, such as the Scherrer method, estimate crystallite size based on peak broadening. However, more advanced line profile analysis methods [5], including the Williamson–Hall (W-H) models, Size–Strain Plot (SSP) method, and Halder–Wagner (H-W) approach, allow for a comprehensive evaluation of size and strain effect broadening, providing deeper insights into the microstructural evolution of the material. ZnTe and Mn-doped ZnTe thin films were produced for this investigation, and XRD analysis was utilized to methodically examine their structural characteristics [6]. Several models were used to assess the crystallite size, microstrain, internal stress, and deformation energy density, including the Scherrer technique, W-H models, SSP, and H-W approaches. A thorough grasp of how Mn doping affects the microstructural character of ZnTe is provided by the comparative analysis, which is essential for their use in next-generation optoelectronic and spintronic devices.

2. Experimental

2.1. Materials

Zinc acetate, tellurium dioxide, ethylene glycol, manganese acetate, sodium hydroxide, sodium borohydride, ammonia, and the glass substrate were procured from Sigma-Aldrich.

2.2. Sample preparation

For the preparation of the thin film from the chemical bath, zinc acetate was used as the source of Zn^{2+} ions, while tellurium dioxide was used as the source of Te^{2-} ions [7]. Ethylene Glycol was used as the solvent, which also served as the complexing agent to control the release of metal ions into the solution. Now, 0.1M of zinc acetate was dissolved in 20 ml of ethylene glycol under continuous magnetic stirring at 140–150°C (Solution A). Besides, 0.1M of tellurium dioxide was separately dissolved in 20ml of ethylene glycol with gentle heating, stirring, and adding sodium hydroxide into the solution until a clear solution was obtained (Solution B). Solution A was then added to Solution B and stirred continuously; thereafter, 40 mg of $NaBH_4$ was added, and then a clean glass substrate was inserted vertically into the reaction bath.

The chemical bath deposition was carried out at 150°C for 90 minutes. The pH of the solution was maintained around 9 by adding a few drops of ammonia solution. After deposition, the glass substrates were taken out, washed with deionized water, and dried at room temperature. For the preparation of Mn-doped ZnTe samples, a 0.001 M concentration of manganese acetate was supplemented into Solution A before mixing with the tellurium source [8].

2.3. Measurements

The structural characteristics of the as-deposited thin films were systematically investigated using the X-ray diffraction (XRD) technique. The XRD measurements were carried out employing a Rigaku MiniFlex 600 X-ray diffractometer equipped with a CuKα radiation source (λ = 1.5406 Å). The XRD patterns were recorded over a 2θ scanning range of 20°–70°, which is sufficient to identify the crystalline phases, preferred crystallographic orientations, and structural quality of the deposited films.

3. Results and discussion

Figure 1 depicts the XRD profile of the un-doped and Mn-doped ZnTe thin films, which revealed distinct diffraction peaks at 25.42°, 29.6°, 42.5°, 49.4°, and 66.5° with miller indices of (111), (200), (220), (311)and (331) planes of cubic zinc blende ZnTe (JCPDS card No. 15-0746), confirming the polycrystalline nature of the prepared films [1, 4]. No secondary phases such as Te, Zn, or Mn compounds were detected, indicating the phase purity of the deposited films.

Also, upon Mn-doping, the same set of peaks was observed, suggesting that Mn ions were effectively integrated into the ZnTe lattice without altering the fundamental cubic structure. However, a slight shift of the peaks toward lower 2θ angles was noticed upon incorporating Mn into ZnTe, implying lattice expansion due to the interchange of Zn^{2+} ions (~0.74 Å) with slightly larger Mn^{2+} ions (~0.80 Å).

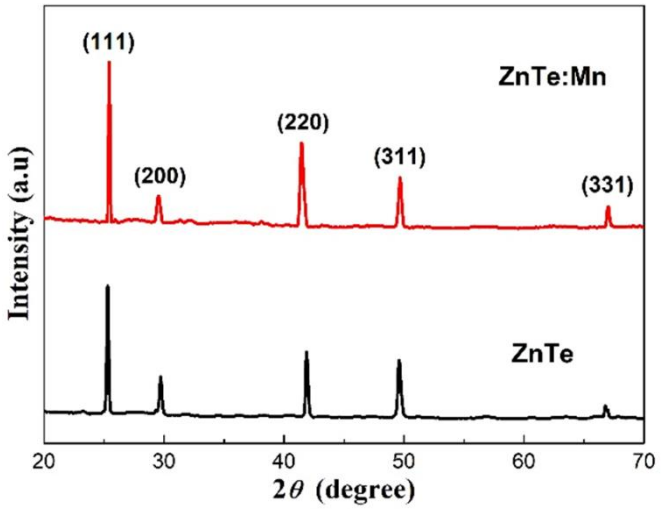

Figure 1. Room-temperature XRD profiles of ZnTe and Mn-doped ZnTe films.

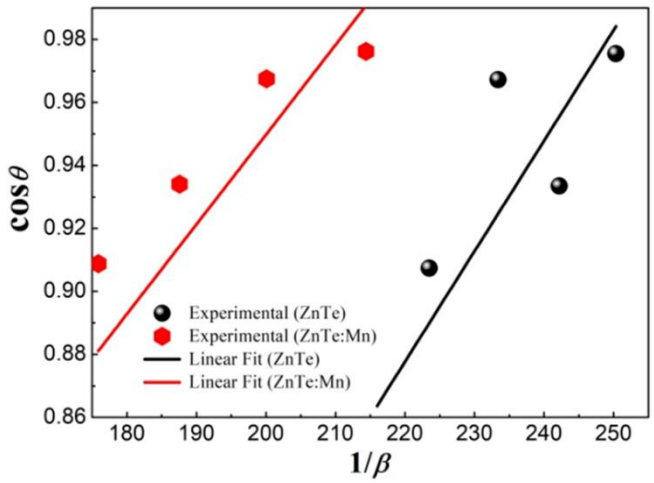

Figure 2. Scherrer plot of ZnTe and Mn-doped ZnTe films.

The crystallite size of ZnTe and Mn-doped ZnTe thin films was estimated using XRD data through the application of the Scherrer equation. The Scherrer formula is given by [9]:

$$D = \frac{0.9\lambda}{\beta_d} \cdot \frac{1}{cos\theta} \quad (1)$$

β_d is the effective broadening corrected for instrumental effects, calculated by [9]:

$$\beta_d = \beta_m^2 - \beta_i^2 \quad (2)$$

β_m is the measured broadening, and β_i is the instrumental broadening determined using a standard silicon sample. Plotting $1/\beta$ *vs.* cosθ, as seen in Figure 2, allows one to determine the average particle size based on the curve's slope, which comes out to be 38 nm and 29 nm. The calculated crystallite sizes are summarized in Table 1.

The crystallite size of ZnTe and Mn-doped ZnTe thin films was evaluated using the modified Scherrer approach by taking the logarithm of equation (1) incorporating instrumental broadening corrections for improved accuracy. XRD patterns were analyzed, and peak profiles were fitted using a pseudo-Voigt function to accurately determine the FWHM [10]. When plotting lnβ − ln(1/cosθ), ln(kλ/D) is obtained at the graph's intersection with the Y-axis.

We call this graph the modified Scherrer graph Figure 3. As a result, one may compute the average crystal size of ZnTe and Mn-doped ZnTe samples. The calculated crystallite sizes are summarized in Table 1. The standard Scherrer equation (3) was modified by taking the logarithm of equation (1) [11]:

$$ln\beta_d = ln\frac{k\lambda}{D} + ln1/cos\theta \quad (3)$$

The pure ZnTe thin film exhibited a crystallite size of approximately 41 nm after the modified modern method, while Mn-doped ZnTe films showed a reduced size of approximately 32 nm. The reduction in crystallite size upon Mn doping suggests the generation of additional lattice imperfections and internal strain, limiting the growth of crystallites.

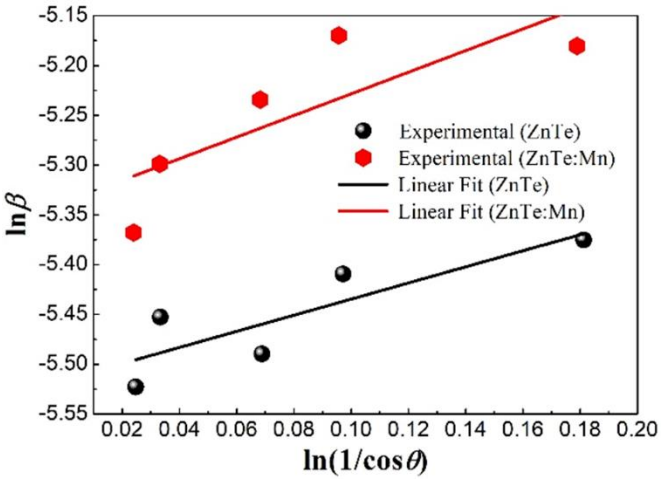

Figure 3. Modern Scherrer plot of ZnTe and Mn-doped ZnTe films.

Table 1. Crystallite size of ZnTe and Mn-doped ZnTe thin films

Sample	2θ (°)	FWHM (°)	Crystallite size (SM); nm	Crystallite size (MSM); nm
ZnTe	25.42	0.229	38	41
Mn-doped ZnTe	25.04	0.267	29	32

The Williamson–Hall method was employed to qualitatively assess the contributions of microstrain. The microstructural parameters of ZnTe and Mn-doped ZnTe thin films were systematically investigated using three W-H-based models: Uniform Deformation Model (UDM), Uniform Stress Deformation Model (USDM), and Uniform Deformation Energy Density Model (UDEDM). This model assumes that the strain is uniformly distributed in all crystallographic directions, and the broadening of the XRD peaks is attributed to both the crystallite size and the lattice strain. The W-H equation based on the UDM is given by [9, 11]:

$$\beta_{total} = \beta_{size} + \beta_{strain} \quad (4)$$

$$\beta_{strain} = 4\epsilon tan\theta \quad (5)$$

So,

$$\beta_{hkl} = \frac{k\lambda}{Dcos\theta} + C \quad (6)$$

On rearranging,

$$\beta_{hkl}cos\theta = \frac{k\lambda}{D} + 4\epsilon sin\theta \quad (7)$$

β_{hkl} is the full width at half of the maximum intensity. In this method, $\beta_{hkl}\cos\theta$ is plotted against $4\sin\theta$ (Figure 4). The intercept of the linear fit yields the crystallite size D, while the slope provides the value of the microstrain ε. The extracted microstructural parameters are summarized in Table 2. The crystallite size estimated from the UDM is consistent with that obtained from the corrected Scherrer method, with a slight reduction due to the consideration of microstrain contributions. The pure ZnTe thin film exhibits a microstrain of approximately 0.8×10^{-3}, while the Mn-doped ZnTe thin film shows an increased microstrain of 1.2×10^{-3}. The increase in microstrain upon Mn doping can be attributed to the substitution of Zn^{2+} ions (0.74 Å) by Mn^{2+} ions (0.80 Å), leading to localized lattice distortions. The enhanced strain not only affects the structural properties but may also influence the optical and magnetic behavior of the films.

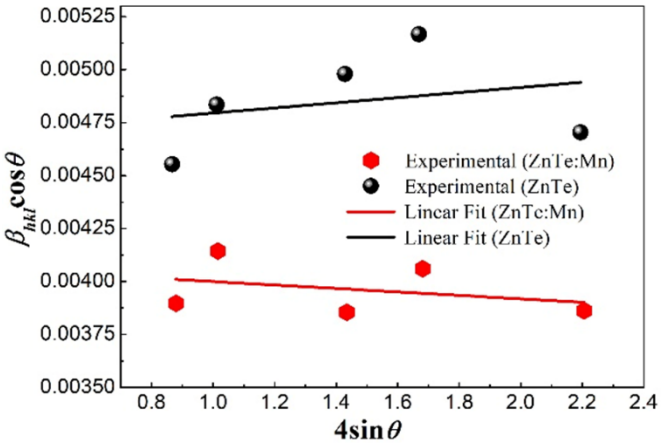

Figure 4. UDM plot of ZnTe and Mn-doped ZnTe films.

To achieve an in-depth understanding of the stress-induced broadening mechanisms in ZnTe and Mn-doped ZnTe thin films, USDM was applied. The USDM is an extension of the W-H analysis, which considers the strain as a result of uniform external or internal stress within the crystal lattice. In USDM, the W-H equation is modified as [9, 11, 12]:

$$\beta_{hkl}cos\theta = \frac{k\lambda}{D} + 4\sigma sin\theta \quad (8)$$

where,

$$\sigma = \epsilon * 1/Y_{hkl} \quad (9)$$

Y_{hkl} is the Young's modulus of the material in the direction of the diffraction vector. For cubic ZnTe, Y_{hkl} along a specific crystallographic direction (hkl) can be calculated using the elastic constants C_{11}, C_{12}, and C_{44}. For the (hkl) direction, Y_{hkl} is given by [9]:

$$\frac{1}{Y_{hkl}} = S_{11} - 2\left[(S_{11} - S_{12}) - \frac{1}{2} * S_{44}\right]\left[\frac{h^2k^2 + k^2l^2 + l^2h^2}{h^2 + k^2 + l^2}\right] \quad (10)$$

where S_{ij} are the elastic compliances, which are inversely related to the elastic constants.

$$S_{11} = \frac{C_{11} + C_{12}}{(C_{11} - C_{12})(C_{11} + 2C_{12})} \quad (11)$$

Table 2. UDM analysis of ZnTe and Mn-Doped ZnTe thin films

Sample	Crystallite size (D, nm)	Microstrain (ε × 10^{-3})
ZnTe	46	0.8
Mn-doped ZnTe	39	1.2

$$S_{12} = \frac{-C_{12}}{(C_{11}-C_{12})(C_{11}+2C_{12})} \quad (12)$$

$$S_{44} = \frac{1}{C_{44}} \quad (13)$$

Cubic ZnTe has the elastic constants C_{11}, C_{12}, and C_{44} of 71.70 GPa, 40.70 GPa, and 31.20 GPa, respectively [13, 14]. By putting the value of elastic constants in equations (11-13), we get the value of elastic compliances 2.36×10^{-2}, -8.58×10^{-3}, and 3.3×10^{-2} GPa^{-1}. Using these values, the calculated Young's modulus for ZnTe (111), (200), (220), (311), and (331) is 131.57 GPa, 42.37 GPa, 25.77 GPa, 33.11 GPa and 71.99 GPa and for Mn-doped ZnTe is 131.60 GPa, 42.5 GPa, 25.9 GPa, 33.44 GPa and 72.04 GPa respectively, the average Young modulus values of ZnTe and Mn doped ZnTe is 60.96 GPa and 61.09 GPa.

In Figure 5, a graph of $\beta_{hkl}\cos\theta$ versus $4\sin\theta/Y_{hkl}$ is plotted. The slope yields the stress σ, while the Y-intercept provides the crystallite size. The extracted parameters are summarized in Table 3. The USDM analysis revealed that Mn doping results in an increased internal stress within the ZnTe lattice. While the undoped ZnTe film exhibited a relatively low compressive stress of 1.03 MPa, the Mn-doped ZnTe thin film exhibited a significantly higher stress value of approximately 1.3 MPa. The enhanced stress is attributed to the lattice mismatch caused by the substitution of Zn^{2+} with slightly larger Mn^{2+} ions and the resulting generation of point defects and dislocations. The observed broadening of the diffraction peaks and the decrease in crystallite size are supported by the increase in internal stress. Because they affect the mechanical stability, as well as optical transitions, and also electrical characteristics of ZnTe-based thin films, these stress-induced effects are crucial, particularly for applications in spintronics and optoelectronics. The excellent linear fit for both samples indicates that the USDM provides an adequate description of the strain broadening mechanism in these films.

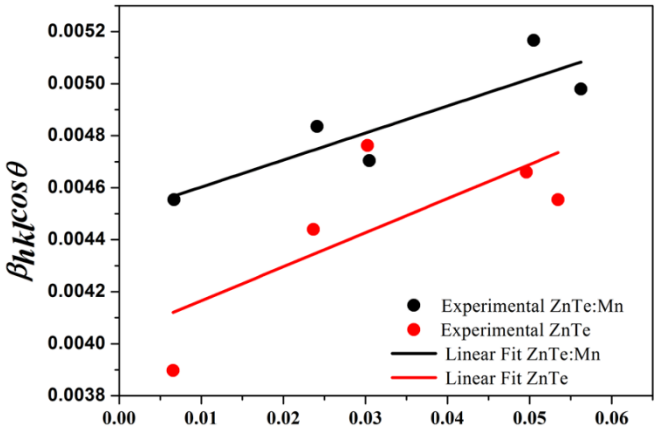

Figure 5. USDM plot of ZnTe and Mn-doped ZnTe films.

Table 3. USDM-based crystallite size and stress in ZnTe and Mn-Doped ZnTe thin films

Sample	Crystallite size (D, nm)	Stress σ (MPa)	R^2 (Fit quality)
ZnTe	45	1.03	0.992
Mn-doped ZnTe	40	1.3	0.995

To gain a more comprehensive understanding of the lattice imperfections and their effect on the mechanical stability of ZnTe and Mn-doped ZnTe thin films, UDEDM was employed. The UDEDM is an extension of the W-H method, where the strain broadening is related to the deformation energy density (u) within the material. The UDEDM-modified W-H equation is given by [11]:

$$\beta_{hkl}cos\theta = \frac{k\lambda}{D} + 4\sigma sin\theta\sqrt{\frac{2u}{Y_{hkl}}} \quad (14)$$

Here, u is the energy density expressed as:

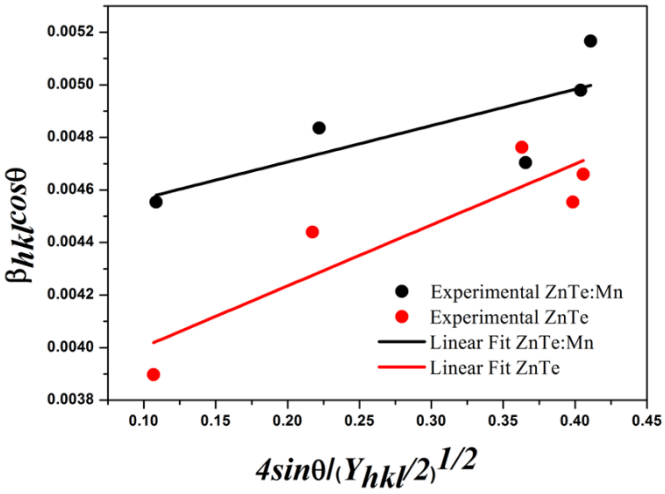

Figure 6. UDEDM plot of ZnTe and Mn-doped ZnTe films.

Table 4. UDEDM-based crystallite size and energy density in ZnTe and Mn-doped ZnTe films

Sample	Crystallite size (D, nm)	Energy Density (u) (kJ/m^3)	R^2 (Fit quality)
ZnTe	44	1.38	0.993
Mn-doped ZnTe	37	2.32	0.992

$$u = \varepsilon^2 . Y_{hkl}/2 \quad (15)$$

In Figure 6, a plot of $\beta_{hkl}\cos\theta$ versus $4\sin\theta\sqrt{2u/Y_{hkl}}$ was constructed. The slope of the linear fit gives the value of energy density, while the intercept provides the crystallite size. According to the investigation, Mn doping resulted in a considerable rise in the deformation energy density. The Mn-doped ZnTe thin film had a greater energy density of 2.32 kJ/m³ than the ZnTe thin film, which had an energy density of 1.38 kJ/m³. Table 4 provides a summary of the extracted parameters. This rise is explained by the inclusion of more point defects, dislocations, and lattice distortions brought about by the addition of Mn ions to the ZnTe crystal lattice. Greater accumulation of elastic strain energy is indicated by the higher energy density seen in Mn-doped ZnTe films, indicating increased internal stresses that may affect the optical, magnetic, and mechanical characteristics of the thin films. Moreover, the decrease in crystallite size observed in Mn-doped ZnTe, compared to pure ZnTe, further supported the presence of lattice distortion and defect-induced stress fields. The high linear correlation coefficients confirm the validation of the UDEDM model in describing the energy-strain relationship in these thin films.

The SSP method was employed to further refine the assessment of the crystallite size and is more reliable than the conventional W-H method [15, 16], as it assumes that the strain broadening has a Lorentzian distribution, while the size broadening has a Gaussian distribution. The SSP equation can be expressed as [9, 11, 17]:

$$(d_{hkl}.\beta_{hkl}cos\theta)^2 = \frac{k\lambda}{D}(d_{hkl}^2.\beta_{hkl}cos\theta) + \frac{\varepsilon^2}{4} \quad (16)$$

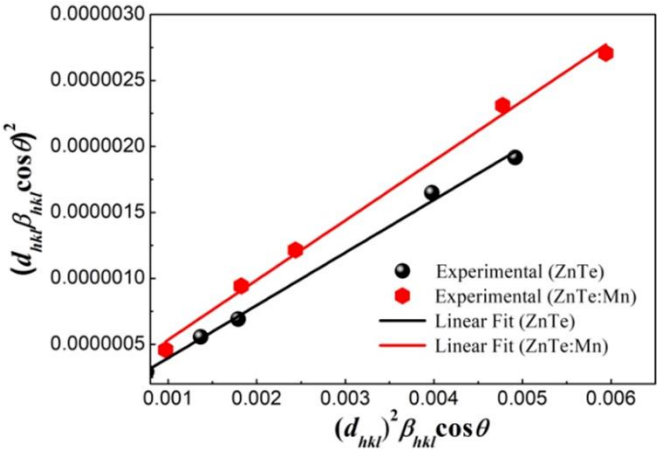

Figure 7. SSP plot of ZnTe and Mn-doped ZnTe films.

Here,

$$d_{hkl}^2 = \frac{a^2}{h^2+k^2+l^2} \quad (17)$$

In Figure 7, a plot of $d_{hkl}^2.\beta_{hkl}cos\theta$ versus $(d_{hkl}.\beta_{hkl}cos\theta)^2$ is drawn. The Y-intercept gives the intrinsic strain, and the slope of the resulting straight line gives the crystallite size. The outcomes of the SSP analysis agree with those derived from the above models based on W-H. When Mn is added, the crystallite size decreases from 42 nm (ZnTe) to 35 nm (Mn-doped ZnTe). This reduction implies that Mn doping results in smaller crystallites by causing lattice deformation and limiting grain development. Furthermore, Mn-doped ZnTe thin films exhibit an increase in microstrain from 1.95×10^{-3} to 2.45×10^{-3}. The extracted parameters are summarized in Table 5. The increment in microstrain is due to the substitutional incorporation of Mn ions into the ZnTe matrix, which causes local lattice distortions due to differences in ionic radii and bonding characteristics. The SSP analysis provides strong evidence that Mn doping significantly influences the crystallographic structure and induces higher internal strain in ZnTe thin films, which can play a vital role in modifying their functional properties.

The H-W approach was used to precisely analyze the crystallite size and microstrain of ZnTe and Mn-doped ZnTe thin films in addition to standard W–H and SSP investigations. For the samples where both effects are important, the H-W technique is more dependable since it assumes a Gaussian distribution for the size component of peak broadening and a Lorentzian distribution for the strain component. The H–W equation is given as [15, 16]:

$$\left(\frac{\beta_{hkl}^*}{d_{hkl}^*}\right)^2 = \frac{1}{D}.\left(\frac{\beta_{hkl}^*}{d_{hkl}^{*2}}\right) + \left(\frac{\varepsilon}{2}\right)^2 \quad (18)$$

Here,

$$\beta_{hkl}^* = \beta_{hkl}cos\theta/\lambda \quad (19)$$

and,

$$d_{hkl}^* = 2d_{hkl}.sin\theta/\lambda \quad (20)$$

Table 5. Crystallite size and microstrain in ZnTe and Mn-Doped ZnTe thin films from SSP analysis

Sample	Crystallite size (D, nm)	Microstrain ($\times 10^{-3}$)	R^2 (Fit quality)
ZnTe	51	1.62	0.991
Mn-doped ZnTe	43	1.83	0.994

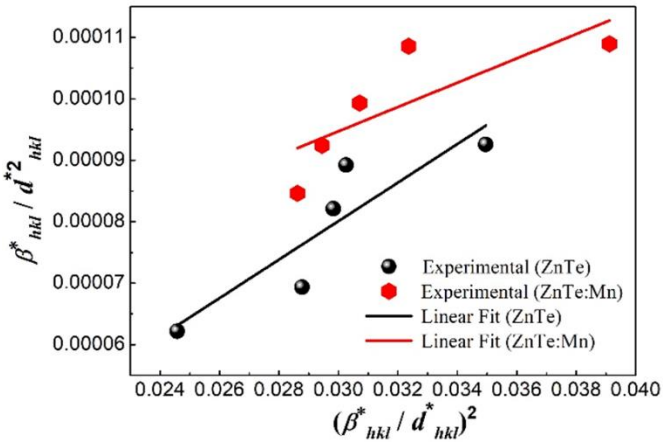

Figure 8. Halder-Wagner plot of ZnTe and Mn-doped ZnTe films.

Table 6. Crystallite size and microstrain in ZnTe and Mn-Doped ZnTe thin films from H-W analysis

Sample	Crystallite size (D, nm)	Microstrain ($\times 10^{-3}$)	R^2 (Fit quality)
ZnTe	45	1.39	0.997
Mn-doped ZnTe	37	3.25	0.995

In Figure 8, the $\beta^*_{hkl}/d^{*^2}_{hkl}$ versus $(\beta^*_{hkl}/d^*_{hkl})^2$ plot was constructed for both undoped and Mn-doped ZnTe thin films. The slope of the straight line gives crystallite size, while the intercept corresponds to the square of the microstrain. The H-W analysis revealed a decrease in crystallite size from 45 nm for ZnTe thin films to 37 nm for Mn-doped ZnTe thin films. This reduction is consistent with the SSP and W-H models, further confirming that Mn-doping inhibits grain growth by introducing defects and strain fields. Moreover, an increase in microstrain was observed upon Mn-doping, rising from 1.39×10^{-3} for pure ZnTe to 3.25×10^{-3} for Mn-doped ZnTe.

Because Mn ions have different ionic radii than Zn ions, the greater strain values indicate enhanced lattice distortions. The findings show that Mn doping has a major impact on ZnTe thin-film microstructural parameters, which may have an impact on the materials' optical, magnetic, and electrical characteristics. Thus, the H-Wagner approach provided a useful and complementary tool to other line profile research techniques, presenting more proof of the strain-induced alterations brought about by Mn inclusion in ZnTe thin films.

4. Conclusions

ZnTe and Mn-doped ZnTe thin films were effectively produced in this work, and XRD analysis was used to methodically examine their structural characteristics. The successful inclusion of Mn ions into the ZnTe lattice was studied by the XRD patterns, which verified the development of a single-phase cubic zinc blende structure devoid of any secondary phases. Using Scherrer, Williamson-Hall, Size-Strain Plot, and Halder-Wagner techniques, a thorough microstructural analysis showed that as the concentration of Mn-doping increased, the size of the crystallites decreased while lattice strain, internal stress, and deformation energy density increased. Because the Halder-Wagner model took into account both Gaussian and Lorentzian peak broadening, it was able to produce the most accurate estimation of crystallite size and strain. It is anticipated that the structural changes brought about by Mn-doping will significantly affect the optical, electrical, and magnetic characteristics of ZnTe thin films, increasing their applicability for spintronic and optoelectronic applications. In order to maximize the films' performance for device applications, future research will concentrate on establishing a correlation between these structural alterations and their functional characteristics.

Conflict of Interest

The authors declare no conflict of interest.

References

1. S. Adachi, *Zinc Telluride (ZnTe)*, in *Optical Constants of Crystalline and Amorphous Semiconductors*. **1999**, Springer US. p. 473.
2. J. Eilers, et al. Optical Properties of Mn-Doped ZnTe Magic Size Nanocrystals. *The Journal of Physical Chemistry Letters*, **2012**, *3*, 1663.
3. A. Jrad, et al. Effect of manganese concentration on physical properties of ZnS:Mn thin films prepared by chemical bath deposition. *Journal of Materials Science: Materials in Electronics*, **2016**, *28*, 1463.
4. I. Spînulescu-Cabnaru, H. Mayer, and J. Hölzl, *The Crystalline Structure of ZnTe Thin Films*, in *December 1*. **1966**, De Gruyter. p. 769.

5. L. Bimbault, et al. Profile analysis of thin film X-ray diffraction peaks. *Thin Solid Films*, **1996**, *275*, 40.

6. A. Pandey, et al. Structural characterization of polycrystalline thin films by X-ray diffraction techniques. *Journal of Materials Science: Materials in Electronics*, **2021**, *32*, 1341.

7. U. Prasad, et al. Effect of Mn Doping on Electrical and Optical Behavior of Chemically Synthesized ZnTe Thin Film. *Journal of Applied Material Science*, **2026**, *2*, 260203.

8. I.A. Younus, A.M. Ezzat, and M.M. Uonis. Preparation of ZnTe thin films using chemical bath deposition technique. *Nanocomposites*, **2020**, *6*, 165.

9. D. Nath, F. Singh, and R. Das. X-ray diffraction analysis by Williamson-Hall, Halder-Wagner and size-strain plot methods of CdSe nanoparticles- a comparative study. *Materials Chemistry and Physics*, **2020**, *239*, 122021.

10. H. Kafashan. X-ray Diffraction Line Profile Analysis of Undoped and Se-Doped SnS Thin Films Using Scherrer's, Williamson–Hall and Size–Strain Plot Methods. *Journal of Electronic Materials*, **2018**, *48*, 1294.

11. E.A. Tokeser and O. Ozturk. Estimation of microstructural parameters by Williamson–Hall, Halder–Wagner, and size–strain plot methods and magnetic properties of (Cu/Mn) co-doped ZnO nanoparticles. *Journal of Materials Science: Materials in Electronics*, **2023**, *34*, 2075.

12. E.R. Shaaban, et al. Microstructural parameters and optical constants of ZnTe thin films with various thicknesses. *Physica B: Condensed Matter*, **2009**, *404*, 3571.

13. B.H. Lee. Elastic Constants of ZnTe and ZnSe between 77°–300°K. *Journal of Applied Physics*, **1970**, *41*, 2984.

14. J. Sörgel and U. Scherz. Ab initio calculation of elastic constants and electronic properties of ZnSe and ZnTe under uniaxial strain. *The European Physical Journal B*, **1998**, *5*, 45.

15. K. Singh, et al. Determination of Structural Elements of Hydrothermally Synthesized CeO_2 Nanoparticles by Monshi, Williamson–Hall, Halder–Wagner, and Size–Strain Plot Methods, and Effect of Annealing Temperature. *Macromolecular Symposia*, **2024**, *413*, 2400104.

16. S.A. Disha, et al. Calculation of crystallite sizes of pure and metals doped hydroxyapatite engaging Scherrer method, Halder-Wagner method, Williamson-Hall model, and size-strain plot. *Results in Materials*, **2024**, *21*, 100496.

17. P. Karil, et al. Study of structural phase transition and elastic properties of ZnTe semiconducting compound under high pressure. *Materials Today: Proceedings*, **2022**, *54*, 782.